清水建設研究報告
第69号平成11年4月

コンクリート構造物の破壊解析に対する多等価直列相モデルの開発

長谷川　俊昭
（技術研究所）

Development of Multi Equivalent Series Phase Model for Fracture Analysis of Concrete Structures

by **Toshiaki Hasegawa**

Abstract

The Multi Equivalent Series Phase Model is derived as a nonlocal macroscopic constitutive law to describe concrete size effects due to fracture localization. Fracture localization at the microscopic level is modeled using a series phase consisting of fracture and unloading phases. Based on a constant plastic fracture energy law, the stress-strain softening relations of the series phase are converted into those of an equivalent series phase, taking into account the length of the series phase. The load-carrying mechanism of concrete is modeled as a number of equivalent series phases distributed with various orientations in the concrete. It is demonstrated that this model provides good predictions of experimentally obtained size effects on concrete constitutive relations. In finite element analysis using the model, previously reported fractures and size effects in experimental specimens under mixed mode I and II loading are well simulated.

概　要

コンクリートの破壊局所化に起因する寸法効果を記述する非局所型構成則として多等価直列相モデルを開発した。微視的レベルでの破壊局所化が破壊相と除荷相からなる直列相としてモデル化され、直列相の軟化応力－ひずみ関係は、塑性破壊エネルギー一定則に基づいて等価直列相の軟化応力－ひずみ関係に変換される。コンクリートの耐荷メカニズムとしては多数の等価直列相がコンクリート中の様々な方向に分布しているレオロジーモデルが仮定される。本モデルはコンクリートの構成関係の寸法効果実験を良好に再現することができる。また、本モデルを用いた有限要素解析では混合モード荷重下の実験試験体の破壊挙動や寸法効果を精度よくシミュレートできることが示される。

§1. Introduction

Mechanical models and constitutive laws for concrete materials must be able to describe nonlocal softening behavior when we numerically simulate softening fractures and damage localization, which relate to size effects and size dependency. Constitutive laws for continuum mechanics in a narrow sense are regarded as local, while constitutive laws able to describe size effects and nonlocal properties of materials are regarded as nonlocal constitutive laws. The crack band model of Bazant and Oh[1] for nonlinear fracture mechanics is considered a simple, nonlocal constitutive model for tensile cracking (mode I fractures). However, it is not that easy to establish a general nonlocal constitutive model for concrete with applicability to multiaxial stress conditions including compression and shear stresses (rotating principal direction). In this study the Multi Equivalent Series Phase (MESP) Model[2),3)] is derived as a nonlocal constitutive law suitable for describing size effects due to fracture localization in concrete under general multiaxial stress conditions.

§2. Multi Equivalent Series Phase Model

2.1 Fracture Localization at the Microscopic Level

Since the presence of coarse aggregate particles makes concrete a heterogeneous material, fracture localization and strain softening occur at a microscopic level in a relatively stable and distributed manner prior to macroscopic softening fractures. Although these types of microscopic behavior should be described by appropriate micromechanics models, we assume a much simpler mechanical field as shown in Fig. 1(a); distributed microscopic fracture regions are modeled by independent fibers constrained by certain conditions as a means to relate the microscopic and macroscopic levels. When a softening fracture occurs in each fiber, the microscopic fracture localizes into a fracture phase within the fiber while an elastic unloading takes place in the remainder of the fiber (the unloading phase). The result is a microscopic strain localization in which the unloading phase supplies the released elastic energy to the fracture phase once the microscopic peak stress of the fiber is reached. We assume that the stresses in each phase depend on the corresponding strains of the phase, and that there are unique

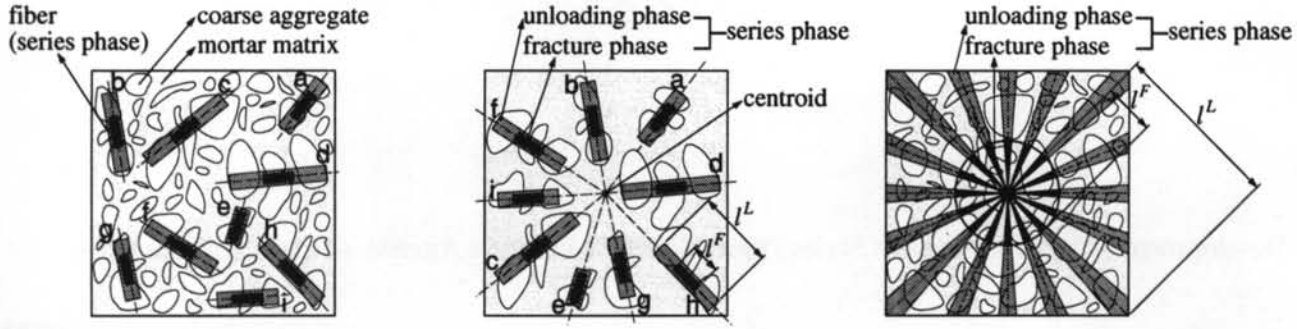

(a) Random distribution of series phases (b) Series phases at the centroid (c) Idealized series phases

Fig. 1 Fracture, unloading, and series phases in a concrete volume element

relations between them that we call phase-constitutive laws. Because of series coupling, the stresses σ^F and σ^U in the fracture and unloading phases are equal. However, the strain ε^U of the unloading phase is much smaller than the strain ε^F of the fracture phase. We define the series phase as the series-coupled combination of the fracture and unloading phases. The strain ε^L of the series phase is calculated from ε^F and ε^U, in which superscripts F, U, and L refer to the fracture, unloading, and series phases. The equilibrium and strain compatibility conditions of the series phase are described by Eq. (1).

$$\sigma^L = \sigma^F = \sigma^U \tag{1a}$$

$$\varepsilon^L = \frac{\varepsilon^F l^F + \varepsilon^U l^U}{l^L} = \frac{\varepsilon^F l^F + \varepsilon^U \left(l^L - l^F\right)}{l^L} \tag{1b}$$

in which l^F, l^U, and l^L are the lengths of the fracture, unloading, and series phases, respectively. This series coupling model consisting of the fracture and unloading phases is considered the basic load-carrying mechanism of concrete at the microscopic level, and the series phase is converted to an equivalent series phase using a simple homogenization method described later.

The MESP Model is a nonlocal macroscopic constitutive model derived assuming that a number of equivalent series phases are distributed with various orientations in the concrete. To derive the model for a concrete volume element, the randomly oriented series phases in the element are collected at the centroid of the element as shown in Fig. 1(b). It is assumed that the length l^L of each series phase is represented by the distance between the centroid and the element boundary, and differs among the series phases (Fig. 1(c)). On the other hand, the length l^F of each fracture phase is the same for all the series phases.

2.2 Equivalent Series Phase

The strain softening response of the series phase has to be composed from the softening behavior of the fracture phase and the elastic unloading behavior of the unloading phase according to the equilibrium and strain compatibility conditions given by Eq. (1). This means that, in general, the stress-strain softening relation for the series phase differs from one direction to another since each series phase has an individual unloading phase length in a concrete volume element. If a macroscopic constitutive model is formulated by composing the softening behavior of the series phase from the fracture and unloading phase responses, it is difficult to satisfy the conditions of Eq. (1) and the calculation becomes inefficient. This is because a kinematic constraint (not a static one) relates the series phase at the microscopic level, rather than the fracture and unloading phases, to the macroscopic level.

The problem is circumvented by introducing an equivalent series phase which is a homogenized phase consisting of the fracture and unloading phases taking the conditions of Eq. (1) into account in a different form. The means of satisfying the equilibrium and strain compatibility conditions of the series phase are to adopt a constant plastic fracture energy law (the first law of thermodynamics) for determining the stress-strain softening relations of the equivalent series phase and to utilize relations similar to those describing the fracture phase for the equivalent series phase.

The stress-strain softening relations (Fig. 2) for the fracture, unloading, and equivalent series phases are assumed as follows. For $0 \le \varepsilon^p \le \varepsilon_0$ (pre-peak):

$$\sigma^p = \sigma_0 \left[1 - \left(1 - \frac{\varepsilon^p}{\varepsilon_0} \right)^{C_0 \varepsilon_0 / \sigma_0} \right] \tag{2a}$$

for $\varepsilon_0 < \varepsilon^p$ (post-peak):

$$\sigma^p = \sigma_0 \exp\left[-\left(\frac{\varepsilon^p - \varepsilon_0}{\varepsilon_s^p} \right) \right] \tag{2b}$$

in which σ^p and ε^p are the stress and strain of phase p; $\varepsilon_0 = \dfrac{\sigma_0}{\zeta C_0}$; and $\varepsilon_s^p = \gamma^p \varepsilon_0 = \dfrac{\gamma^p \sigma_0}{\zeta C_0}$. Superscripts $p = F$, U, and E refer to the fracture, unloading, and equivalent series phases, but Eq. (2b) is not necessary for the unloading phase. In Eq. (2), C_0 is the initial modulus, σ_0 is the peak stress of the curve, ζ is a parameter controlling the peak strain ε_0, and γ^p is

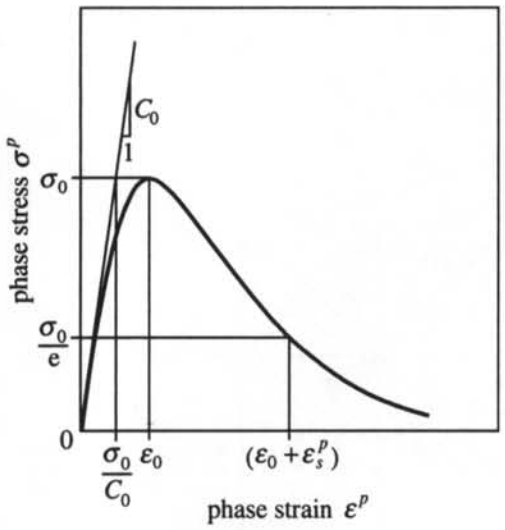

Fig. 2 Stress-strain softening relation for phase

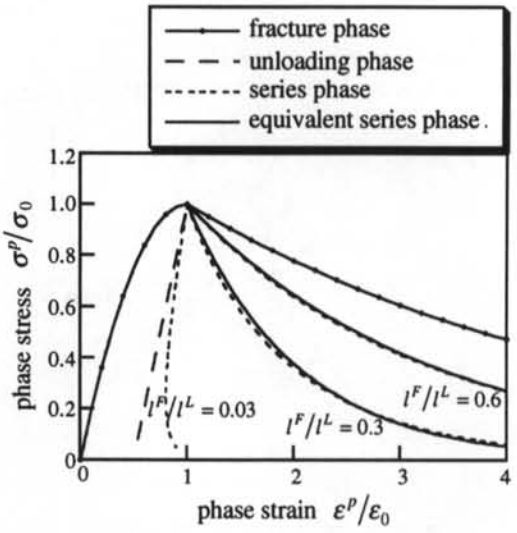

Fig. 3 Strain softening response of each phase

a ductility parameter that controls ε_s^p. At the strain $\varepsilon^p = \varepsilon_0 + \varepsilon_s^p$, the stress σ^p decreases to σ_0/e in the softening region, i.e., the ductility in the softening region depends on the strain ε_s^p or the ductility parameter γ^p. The stress-strain relations in the pre-peak region are the same for all phases, but in the post-peak region the equivalent series phase takes a different value γ^E of ductility parameter from the value γ^F for the fracture phase. On the other hand, the unloading phase follows an elastic unloading path with the initial modulus C_0 after the peak stress.

The constant plastic fracture energy law is written as Eq. (3).

$$V^E\left(l^E\right)g^E = V^F\left(l^F\right)g^F + V^U\left(l^U\right)w^U \tag{3a}$$

$$V^E\left(l^E\right)\int_{\varepsilon^E=0}^{\varepsilon^E=\infty}\sigma^E\,d\varepsilon^E = V^F\left(l^F\right)\int_{\varepsilon^F=0}^{\varepsilon^F=\infty}\sigma^F\,d\varepsilon^F + V^U\left(l^U\right)\left[\int_{\varepsilon^U=0}^{\varepsilon^U=\varepsilon_0}\sigma^U\,d\varepsilon^U - \frac{\sigma_0^2}{2C_0}\right] \tag{3b}$$

in which $V^F\left(l^F\right)$, $V^U\left(l^U\right)$, and $V^E\left(l^E\right)$ are volumes of the fracture, unloading, and equivalent series phases depending on the length of each; g^F and g^E are the plastic fracture energy densities of the fracture and equivalent series phases; and w^U is the plastic energy density of the unloading phase. When parameters C_0 and ζ for the pre-peak region, the ductility parameter γ^F for the fracture phase, and the volume of each phase are given, the ductility parameter γ^E for the equivalent series phase can be determined by solving Eqs. (2) and (3). Furthermore, if the volume of the equivalent series phase is assumed to be the same as the volume of the series phase consisting of the fracture and unloading phases, i.e., Eq. (4), then the solution for γ^E is given by Eq. (5).

$$V^E\left(l^E\right) = V^L\left(l^L\right) = V^F\left(l^F\right) + V^U\left(l^U\right) \tag{4}$$

$$\gamma^E = \frac{V^F\left(l^F\right)}{V^L\left(l^L\right)}\left(\frac{\zeta}{2}+\gamma^F\right) - \frac{\zeta}{2} \tag{5}$$

The volume ratio $V^F\left(l^F\right)/V^L\left(l^L\right)$ in Eq. (5) is estimated using Eq. (6), and $d = 1$ is assumed in this study.

$$\frac{V^F\left(l^F\right)}{V^L\left(l^L\right)} = \left(\frac{l^F}{l^L}\right)^d \tag{6}$$

in which d is a parameter depending on the shape of the series phase; and $d = 1$ or 3 if the series phase is treated as a cylinder with a uniform circular section or as a cone with various circular sections.

In Fig. 3 calculated softening responses of equivalent series phases are compared with those of series phases composed from the behavior of the fracture and unloading phases. These results show that the strain softening response of the equivalent series phase is almost identical to that of the series phase. However, for a snapback as in the case of $l^F/l^L = 0.03$, the equivalent series phase model is not applicable since a kinematic constraint is adopted in the model, as described later.

2.3 Multi Equivalent Series Phase Model

To derive a nonlocal macroscopic constitutive model, i.e., the MESP Model, for the concrete volume element shown in Fig. 4(a), every series phase with its own length l^L between the centroid of the element and the element boundary is replaced with an equivalent series phase. The stress-strain softening relation of each equivalent series phase depends on the length l^L of the series phase, and is determined using Eq. (5).

In each equivalent series phase a normal strain ε_N^E in the direction **n** of the fiber and two shear strains ε_{TK}^E and ε_{TM}^E in the directions of the unit coordinate vectors **k** and **m** are considered. The unit coordinate vectors **n**, **k**, and **m** are normal to one another (Fig. 4(a)). As in the Enhanced

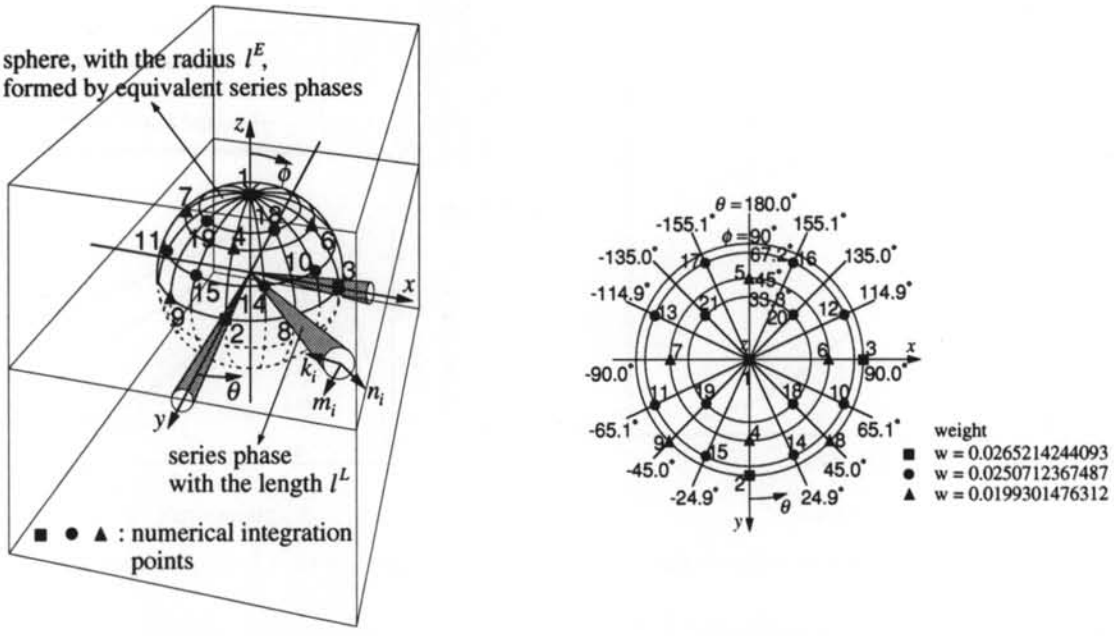

(a) Concrete volume element and sphere (b) Numerical integration points for hemisphere

Fig. 4 Multi equivalent series phases model

Microplane Concrete (EMPC) Model[4),5)] a tensorial kinematic constraint is hypothesized to relate the macroscopic strain tensor ε_{ij} to the strains of the equivalent series phase, i.e., the normal strain ε_N^E and shear strains ε_{TK}^E and ε_{TM}^E of the equivalent series phase are the resolved components of the macroscopic strain tensor ε_{ij}.

$$\varepsilon_N^E = n_i n_j \varepsilon_{ij} \tag{7a}$$

$$\varepsilon_{TK}^E = \frac{1}{2}\left(k_i n_j + k_j n_i\right)\varepsilon_{ij} \tag{7b}$$

$$\varepsilon_{TM}^E = \frac{1}{2}\left(m_i n_j + m_j n_i\right)\varepsilon_{ij} \tag{7c}$$

in which n_i, k_i, and m_i are components of the unit coordinate vectors $\mathbf{n}$, $\mathbf{k}$, and $\mathbf{m}$. In this paper, indicial notation is used for tensors and the Latin lower-case subscripts refer to Cartesian coordinates x_i, $i = 1, 2, 3$ (x, y, z).

Normal stress σ_N^E and shear stresses σ_{TK}^E and σ_{TM}^E of the equivalent series phase mainly depend on the normal strain ε_N^E and shear strains ε_{TK}^E and ε_{TM}^E, respectively. The incremental forms of the phase-constitutive relations for the equivalent series phase are written separately for the normal component and the shear components in the K and M directions:

normal component:
$$d\sigma_N^E = C_N^E d\varepsilon_N^E - d\sigma_N^{E''} = f_{N1}^E\left(\varepsilon_N^E, \varepsilon_L^E, S_L^E\right) \tag{8a}$$

K-shear component:
$$d\sigma_{TK}^E = C_{TK}^E d\varepsilon_{TK}^E - d\sigma_{TK}^{E''} = f_{T1}^E\left(\varepsilon_{TK}^E, S_N^E\right) \tag{8b}$$

M-shear component:
$$d\sigma_{TM}^E = C_{TM}^E d\varepsilon_{TM}^E - d\sigma_{TM}^{E''} = f_{T1}^E\left(\varepsilon_{TM}^E, S_N^E\right) \tag{8c}$$

in which C_N^E, C_{TK}^E, and C_{TM}^E = incremental elastic stiffnesses for the equivalent series phase; $d\sigma_N^{E''}$, $d\sigma_{TK}^{E''}$, and $d\sigma_{TM}^{E''}$ = inelastic stress increments for the equivalent series phase; $f_{N1}^E\left(\varepsilon_N^E, \varepsilon_L^E, S_L^E\right)$ = normal stress increment $d\sigma_N^E$ expressed in terms of normal strain ε_N^E, the resolved lateral strain ε_L^E of the macroscopic strain tensor ε_{ij}, and the resolved lateral stress S_L^E of the macroscopic stress tensor σ_{ij} onto the phase; and $f_{T1}^E\left(\varepsilon_{Ts}^E, S_N^E\right)$ = shear stress increment $d\sigma_{Ts}^E$ expressed in terms of shear strain ε_{Ts}^E and the resolved normal stress S_N^E of the macroscopic stress tensor σ_{ij} onto the phase $(Ts = TK, TM)$.

Since a uniform state of macroscopic stress and strain is assumed in the concrete volume element, and microscopic softening localization is homogenized using the equivalent series phase, with the length of the series phase taken into account, we can use an arbitrary inner volume within the element to relate the responses of the equivalent series phases to the macroscopic behavior. Here a sphere, with a radius l^E, formed by the equivalent series phases is considered (Fig. 4(a)). Using the principle of virtual work (i.e., the equality of virtual works δW^V of the macroscopic stress tensor and δW^E of the stresses in the equivalent series phases within the sphere of radius l^E), we can write

$$\delta W^V = \delta W^E \tag{9a}$$

$$\delta W^V = \int_{r=0}^{r=l^E}\int_{\theta=0}^{\theta=2\pi}\int_{\phi=0}^{\phi=\pi} d\sigma_{ij}\delta\varepsilon_{ij}\, r^2 \sin\phi\, d\phi\, d\theta\, dr = \frac{4}{3}\pi\left(l^E\right)^3 d\sigma_{ij}\delta\varepsilon_{ij} \tag{9b}$$

$$\delta W^E = \int_{\theta=0}^{\theta=2\pi}\int_{\phi=0}^{\phi=\pi}\left(d\sigma_N^E\delta\varepsilon_N^E + d\sigma_{TK}^E\delta\varepsilon_{TK}^E + d\sigma_{TM}^E\delta\varepsilon_{TM}^E\right) \cdot\frac{1}{3} f(\mathbf{n})\left(l^E\right)^3 \sin\phi\, d\phi\, d\theta \tag{9c}$$

in which θ and ϕ = the spherical angular coordinates (Fig .4); and $\delta\varepsilon_{ij}$, $\delta\varepsilon_N^E$, $\delta\varepsilon_{TK}^E$, and $\delta\varepsilon_{TM}^E$ = small variations of the strain tensor and of the phase strains. The function $f(\mathbf{n})$ is a weight function for the fiber directions $\mathbf{n}$, which in general can be used to introduce anisotropy of the material in its initial state. We will use $f(\mathbf{n}) = 1$, which means isotropy. In this study, two series phases with opposite orientations in the upper $(0 \le \phi \le \pi/2)$ and lower $(\pi/2 < \phi \le \pi)$ hemispheres are replaced, for simplicity, by a single series phase which is the average of their lengths. Then Eq. (9) is reduced to a directional integration over the upper hemisphere.

$$\frac{4}{3}\pi\left(l^E\right)^3 d\sigma_{ij}\delta\varepsilon_{ij} = \frac{2}{3}\left(l^E\right)^3 \int_{\theta=0}^{\theta=2\pi}\int_{\phi=0}^{\phi=\pi/2}\left(d\sigma_N^E\delta\varepsilon_N^E + d\sigma_{TK}^E\delta\varepsilon_{TK}^E + d\sigma_{TM}^E\delta\varepsilon_{TM}^E\right)f(\mathbf{n})\sin\phi\, d\phi\, d\theta \quad (10)$$

Expressing $\delta\varepsilon_N^E$, $\delta\varepsilon_{TK}^E$, and $\delta\varepsilon_{TM}^E$ by Eq. (7), and substituting them into Eq. (10) along with the phase-constitutive relations Eq. (8), we obtain an incremental form of the macroscopic stress-strain relation

$$d\sigma_{ij} = C_{ijrs}d\varepsilon_{rs} - d\sigma_{ij}^{''} \quad (11a)$$

$$C_{ijrs} = \eta\int_{\theta=0}^{\theta=2\pi}\int_{\phi=0}^{\phi=\pi/2}\left[n_i n_j n_r n_s C_N^E + \frac{1}{4}\left(k_i n_j + k_j n_i\right)\left(k_r n_s + k_s n_r\right)C_{TK}^E + \frac{1}{4}\left(m_i n_j + m_j n_i\right)\left(m_r n_s + m_s n_r\right)C_{TM}^E\right] \cdot f(\mathbf{n})\sin\phi\, d\phi\, d\theta \quad (11b)$$

$$d\sigma_{ij}^{''} = \eta\int_{\theta=0}^{\theta=2\pi}\int_{\phi=0}^{\phi=\pi/2}\left[n_i n_j d\sigma_N^{E''} + \frac{1}{2}\left(k_i n_j + k_j n_i\right)d\sigma_{TK}^{E''} + \frac{1}{2}\left(m_i n_j + m_j n_i\right)d\sigma_{TM}^{E''}\right]\cdot f(\mathbf{n})\sin\phi\, d\phi\, d\theta \quad (11c)$$

in which $\eta = \eta^E$; and $\eta^E = 1/2\pi$.

The EMPC Model is a local constitutive model derived by treating microscopic fracture regions as planes (microplanes) of various orientations. The constitutive equation for the EMPC Model results in a surface integral over a unit hemisphere with a surface consisting of microplanes, and is obtained in the form of Eq. (11) with $\eta = \eta^M = 3/2\pi$ by replacing C_N^E, C_{TK}^E, C_{TM}^E, $d\sigma_N^{E''}$, $d\sigma_{TK}^{E''}$, and $d\sigma_{TM}^{E''}$ with the corresponding variables for the microplanes. In the study of the EMPC Model, analytical expressions for the initial normal and shear moduli C_{N0}^M and C_{T0}^M of a microplane are obtained by substituting C_{N0}^M and C_{T0}^M for the incremental elastic stiffnesses in Eq. (11b), considering initial isotropic elasticity. Initial normal and shear moduli C_{N0}^E and C_{T0}^E of the equivalent series phase can be obtained for the MESP Model using a similar method. These initial moduli for both models are

$$C_{N0}^M = \frac{E_0}{(1-2\nu_0)} = \frac{1}{3}C_{N0}^E \quad (12a)$$

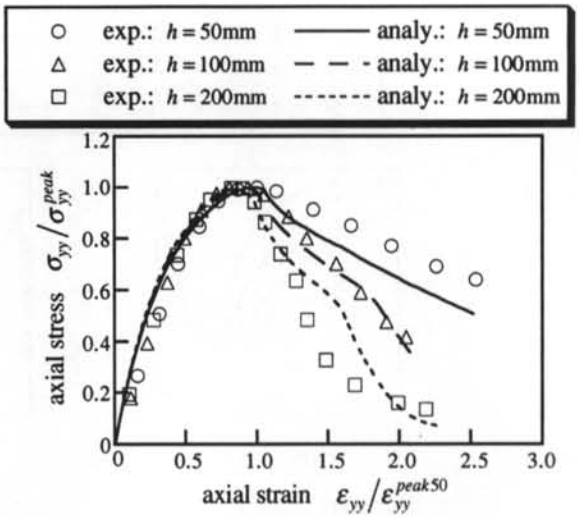

Fig. 5 Uniaxial compression analysis

$$C_{T0}^M = \frac{(1-4\nu_0)E_0}{(1-2\nu_0)(1+\nu_0)} = \frac{1}{3}C_{T0}^E \quad (12b)$$

in which E_0 and ν_0 are Young's modulus and Poisson's ratio. If we redefine the initial moduli of the equivalent series phase as $C_{N0}^E \equiv C_{N0}^M$ and $C_{T0}^E \equiv C_{T0}^M$, and set $\eta = \eta^M = 3/2\pi$ in Eq. (11), the microconstitutive models for microplanes in the EMPC Model can be utilized as phase-constitutive models for the fracture phases in the MESP Model, which is a very attractive approach since the EMPC Model has succeeded in describing the local constitutive relations of concrete under multiaxial stress conditions with accuracy. We do this in the present study.

The developed MESP Model has been implemented in the several computational programs. The program DMP is a constitutive equation solver to calculate constitutive relations of the model with complicated stress and strain paths. The model has also been implemented in the finite element program DIAMESP based on the general purpose finite element system DIANA[6] for practical and complicated structural calculation.

§ 3. Verification of Constitutive Relations

The developed MESP Model is verified by comparing the calculated results it yields with experimentally obtained size effects on the constitutive relations of concrete as reported in the literature. In each calculation, the size of a concrete volume element in the MESP Model (Fig. 4(a)) is assumed to be the same as the concrete specimen in the corresponding experiment. This verification of the constitutive relations given by the MESP Model is carried out using the constitutive equation solver DMP.

3.1 Uniaxial Compression Analysis

In Fig. 5 the calculated results of the size effect on uniaxial compressive softening are compared with tests by Van Mier[7]

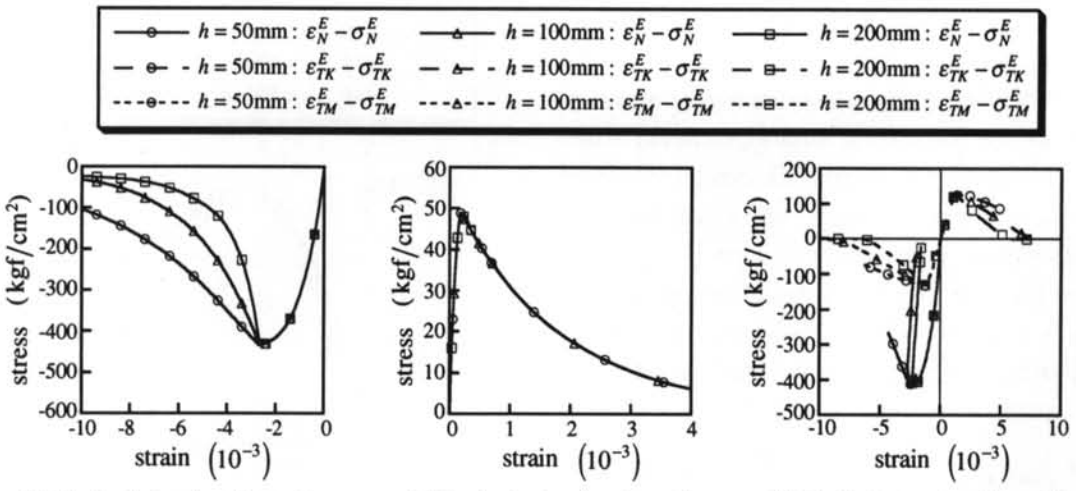

(a) Equivalent series phases 2 (b) Equivalent series phases 3 (c) Equivalent series phases 14

Fig. 6 Responses of equivalent series phases for uniaxial compression analysis

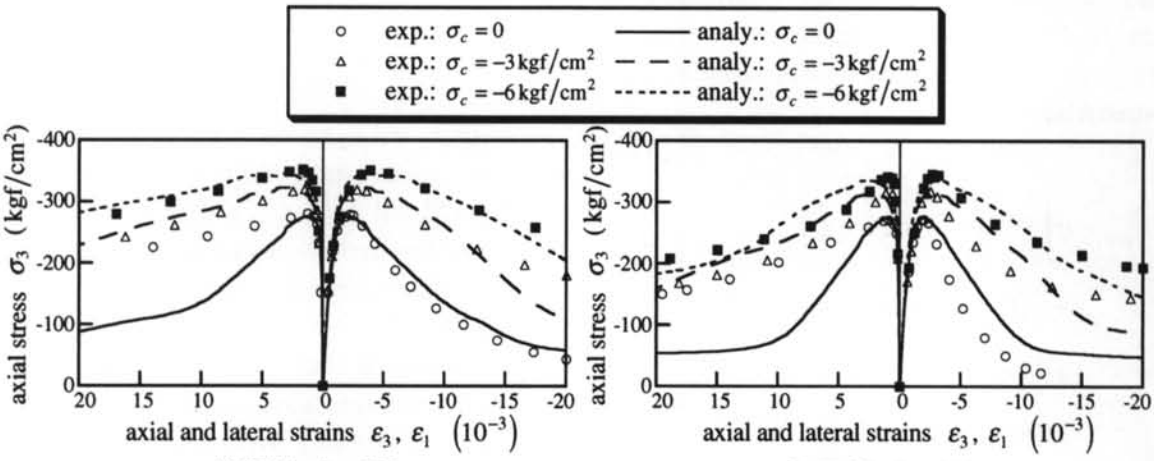

(a) Height $h = 100$ mm (b) Height $h = 200$ mm

Fig. 7 Triaxial compression analysis

using concrete prism specimens of the identical section (100×100 mm) but different heights h (50, 100, and 200 mm). The axial stress-strain relations are normalized by the peak axial stress σ_{yy}^{peak} of each specimen, and the axial strain $\varepsilon_{yy}^{peak50}$ corresponding to the peak axial stress of the specimen with $h = 50$ mm. In the analysis, the length l^F of the fracture phase is assumed to be $2l^F = 50\text{ mm} \cong 3d_{\max} = 48\text{ mm}$, in which $d_{\max}$ is the maximum aggregate size. The MESP Model can capture the decrease in ductility with increasing specimen height. Figure 6 shows the normal, *K*-shear, and *M*-shear responses of equivalent series phases (integration points) 2, 3, and 14 (Fig. 4) in the analysis. The increase in specimen height causes more brittle softening responses of the equivalent series phases, and this results in brittle macroscopic behavior.

3.2 Triaxial Compression Analysis

Figure 7 shows the results of triaxial compression analysis along the compressive meridian in comparison with experiments by Kosaka et al.[8]. In these experiments concrete prism specimens of the identical section (100×100 mm) but different heights h (100 and 200 mm) were tested under confinement pressures σ_c of 0, −3, and −6 kgf/cm^2. The length l^F of the fracture phase is taken to be $2l^F = 100\text{ mm} = 6.6d_{\max}$ in this analysis. Although the analysis underestimates the lateral strain in the softening regime during uniaxial compression as compared with the experimental results, the model roughly predicts the size effects on triaxial compressive softening.

3.3 Biaxial Tension-Shear Analysis

To examine applicability of the model under shear stress with a rotating principal direction, the biaxial tension-shear analysis of Rots[9] is simulated. In this analysis, uniaxial tension up to the uniaxial tensile strength f_t is first applied to a concrete volume element in the x-direction. The element is then immediately subjected to combined biaxial tension and shear according to $\Delta\varepsilon_{xx} : \Delta\varepsilon_{yy} : \Delta\gamma_{xy} = 0.5 : 0.75 : 1$. Two sizes of square element (10×10 mm and 20×20 mm) with thickness

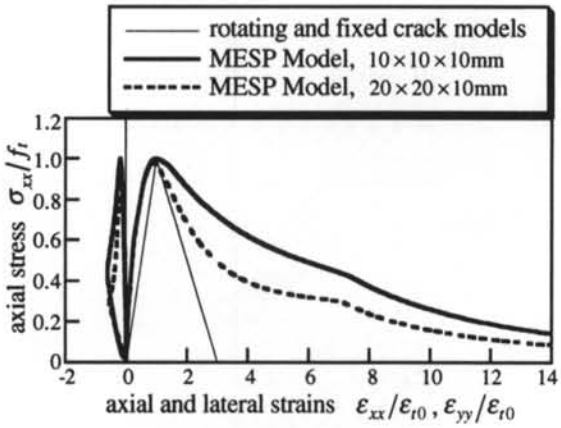

Fig. 8 Uniaxial tension analysis

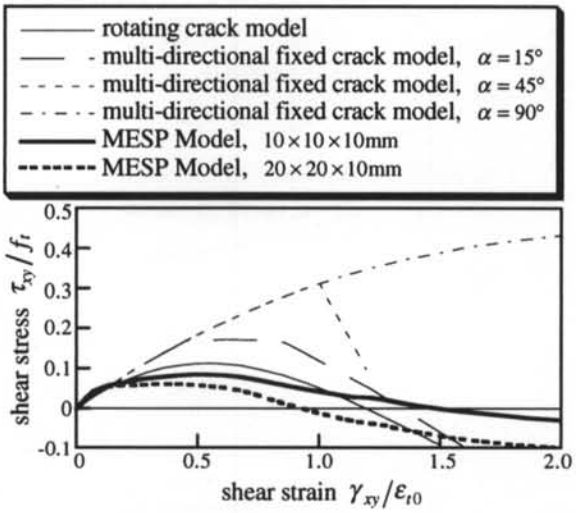

Fig. 9 Shear responses in biaxial tension-shear analysis

10 mm are considered, and the length l^F of the fracture phase is assumed to be $2l^F = 10$ mm in the MESP Model. In Fig. 8, the results of uniaxial tension analysis using the MESP Model prior to the biaxial tension-shear analysis are shown along with the uniaxial tensile relation assumed in the analysis by Rots, who used the rotating crack model and the multi-directional fixed crack model, in which ε_{t0} is the axial strain corresponding to f_t.

In Fig. 9, the shear responses obtained in the biaxial tension-shear analysis using the MESP Model are compared with the results calculated by Rots using the rotating crack model and the multi-directional fixed crack model (α = threshold angle). It is worth noting that the MESP Model predictions of the flexible shear responses for both element sizes are similar to the result achieved with the rotating crack model, which has been shown capable of simulating shear-tension failures of concrete, while the multi-directional fixed crack model, with larger values of α, results in much stiffer shear behavior. The MESP Model can simulate the size effects on shear strength and softening as shown in Fig. 9.

The rotation angles θ_σ and θ_ε of principal stress and strain are shown in Fig. 10 for the element $10\times10\times10$ mm in

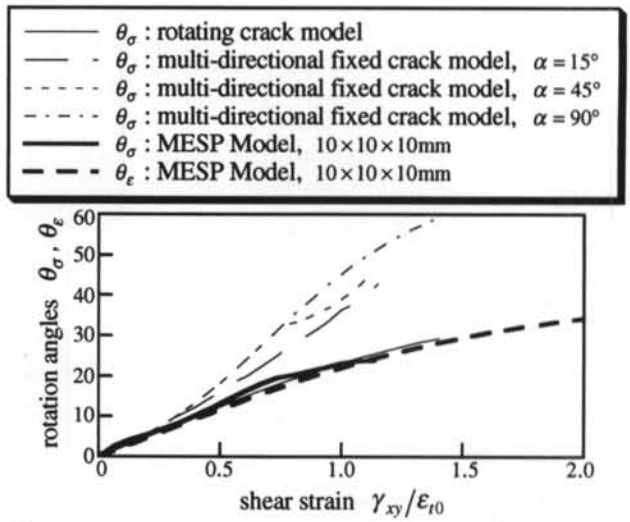

Fig. 10 Rotation of principal axes in biaxial tension-shear analysis

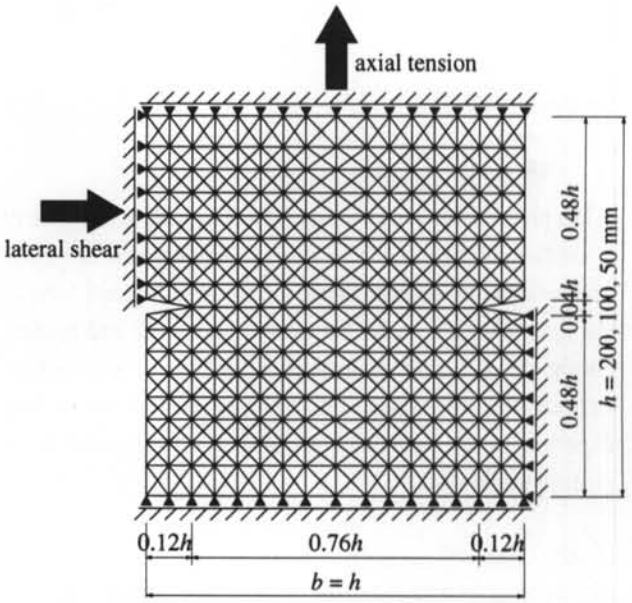

Fig. 11 Finite element modeling of double-edge-notched specimen under shear-tension

comparison with the results obtained by the rotating crack model and the multi-directional fixed crack model. The axes of principal stress and strain coincide in the present analysis, as with the rotating crack model. This means that the MESP Model incorporates the capabilities of the rotating crack model, which has previously been shown effective in its application to fracture mechanics.

§ 4. Verification Using Finite Element Analysis

To verify the applicability of the MESP Model to the fracture analysis of concrete structures, the shear-tension tests carried out by Van Mier and Nooru-Mohamed [10), 11)] on double-edge-notched mortar specimens are simulated using the finite element

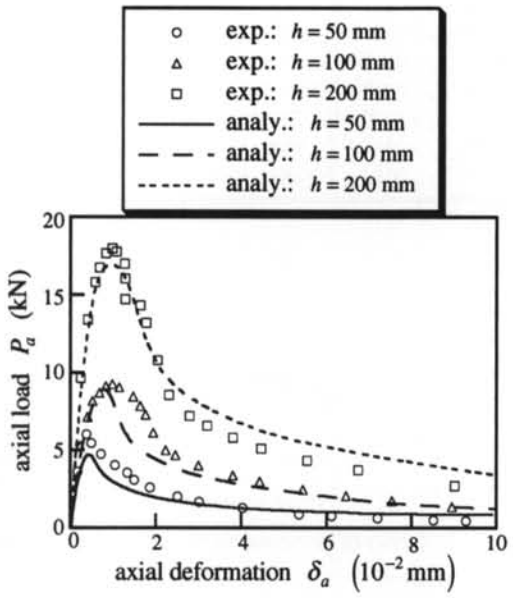

Fig. 12 Axial responses in shear-tension analysis

program DIAMESP.

4.1 Finite Element Modeling

The proportional loading tests of load-path 6b in the work of Van Mier and Nooru-Mohamed are chosen, in which the ratio of axial to lateral deformations was kept at two. Figure 11 shows the finite element mesh, boundary conditions, and loading configuration for the shear-tension analysis. Specimens of heights $h = 50$, 100, and 200 mm in the size effect experiments are modeled with geometrically similar finite element meshes.

4.2 Shear-Tension Analysis

Calculated relations between axial load P_a and deformation δ_a are compared with the corresponding experimental results in Fig. 12. The numerical analysis provides a good prediction of the axial response seen in the experiments, including the size effects on maximum axial load $P_a^{\max}$ as well as softening stiffness.

In Fig. 13, the incremental deformation of the $h = 50$ mm specimen in the finite element analysis is compared with the experimentally observed crack patterns in specimens of heights $h = 50$, 100, and 200 mm. This is at the load step where the axial load P_a decreases to $P_a/P_a^{\max} = 0.2$ in the softening branch. The two overlapping cracks obtained in the numerical analysis are very similar to the cracking observed in the experiments.

Figures 14 and 15 show the analytical distribution of positive maximum principal strain and negative minimum principal stress in the $h = 50$ mm specimen at the same load step. These results indicate that mode I fractures are dominant in specimens with this type of loading path, although the mixed mode type of

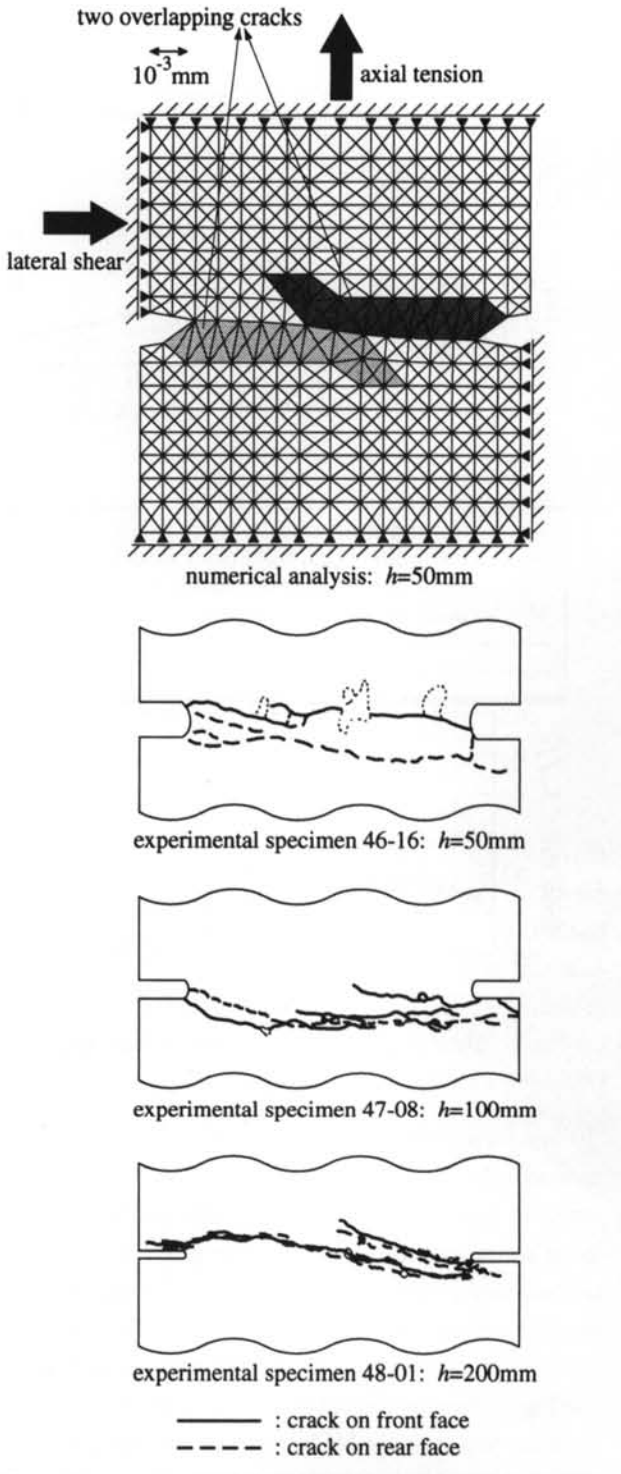

Fig. 13 Incremental deformation in shear-tension analysis compared with experimental crack patterns

loading is applied.

The results of the finite element analysis verify that the MESP Model is able to predict fractures and size effects in concrete structures with accuracy.

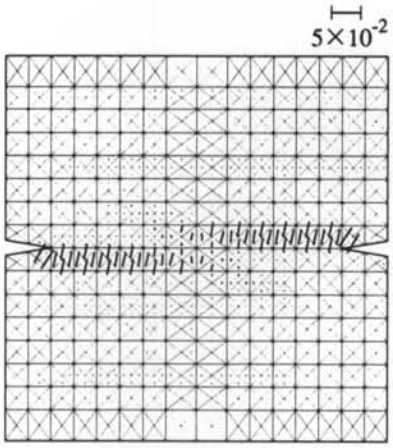

Fig. 14 Distribution of positive maximum principal strain in shear-tension analysis

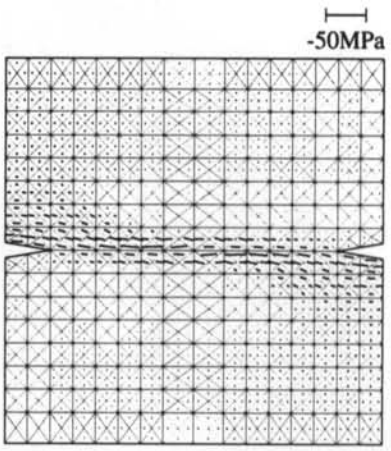

Fig. 15 Distribution of negative minimum principal stress in shear-tension analysis

§ 5. Conclusions

Fracture localization in concrete at the microscopic level has been modeled using a series phase consisting of the fracture and unloading phases, and the softening constitutive relations of this series phase are converted into those of an equivalent series phase using a simple homogenization method. The Multi Equivalent Series Phase Model is derived as a nonlocal macroscopic constitutive model assuming that a number of such equivalent series phases are distributed with various orientations in the concrete. It has been demonstrated that this model provides good predictions of experimentally obtained size effects on concrete constitutive relations. Finite element analysis using the model gives accurate predictions of fractures and size effects in concrete structures.

Acknowledgment

Implementation of the Multi Equivalent Series Phase Model in the finite element program DIAMESP based on the general purpose finite element system DIANA was carried out by the author as a member of DIANA Foundation while he was a visiting researcher at the Netherlands Organization for Applied Scientific Research (TNO). The author would like to acknowledge the staff of TNO for providing him with expertise in programing in DIANA.

References

1) Bazant, Z. P., and Oh, B. H.: "Crack band theory for fracture of concrete", Materiaux et Constructions, Vol. 16, No. 93, pp.155-177, 1983.
2) Hasegawa, T.: "Multi equivalent series phase model for nonlocal constitutive relation of concrete", Proceedings of the 47th Annual Conference of JSCE, Vol. 5, pp.18-19, 1992 (in Japanese).
3) Hasegawa, T.: "Multi equivalent series phase model and nonlocal microplane model for concrete", Proceedings of the 48th Annual Conference of JSCE, Vol. 5, pp.4-5, 1993 (in Japanese).
4) Hasegawa, T.: "Enhanced microplane concrete model", Fracture Mechanics of Concrete Structures, ed. F. H. Wittmann, AEDIFICATIO, pp.857-870, 1995.
5) Hasegawa, T.: "Development and verification of enhanced microplane concrete model", Concrete Library International, JSCE, No. 29, pp.159-202, 1997.
6) "DIANA User's manual - Release 6.1", Building and Construction Research, Netherlands Organization for Applied Scientific Research, 1996.
7) Van Mier, J. G. M.: "Strain-softening of concrete under multiaxial loading conditions", Ph.D. thesis, Eindhoven University of Technology, The Netherlands, 1984.
8) Kosaka, Y., Tanigawa, Y., and Hatanaka, S.: "Evaluation of effect of confinements on compressive toughness of concrete based on triaxial compressive test data", Proceedings of JCI 7th Conference, pp.305-308, 1985 (in Japanese).
9) Rots, J. G.: "Computational modeling of concrete fracture", Ph.D. Thesis, Delft University of Technology, The Netherlands, 1988.
10) Van Mier, J. G. M., Nooru-Mohamed, M. B., and Timmers, G.: "An experimental study of shear fracture and aggregate interlock in cementbased composites", HERON, Vol. 36, No. 4, 1991.
11) Nooru-Mohamed, M. B.: "Mixed-mode fracture of concrete: an experimental approach", Ph.D. Thesis, Delft University of Technology, The Netherlands, 1992.